Electromechanical Design of a 16-T CCT Twin-Aperture Dipole for FCC

Bernhard Auchmann, Lucas Brouwer, Shlomo Caspi, Jiani Gao, Giuseppe Montenero, Marco Negrazus, Gabriella Rolando, and Stéphane Sanfilippo

***Abstract*—Canted-cosine-theta (CCT) technology has been studied for its suitability for a future-circular-collider (FCC) main dipole in terms of magnetic and mechanical performance, electrothermal protectability, as well as efficiency. In this paper, we present lessons learnt from our search for efficient CCT solutions by means of two-dimensional (2-D) magnetic and mechanical simulations, discuss the 3-D periodic mechanical model, as well as 3-D electromagnetic analysis of the end regions. Temperature and voltage distributions during a quench under simplifying assumptions are discussed, and the magnet's efficiency is compared to that of other contenders in the FCC design study. The results qualify the CCT design as a contender for the FCC main dipole.**

***Index Terms*—FCC, CCT, Nb_3Sn accelerator magnet.**

I. Introduction

THE Future-Circular-Collider (FCC) design study investigates, among many other things, feasible designs for the FCC 16-T main dipole magnet using Nb_3Sn technology [1]. Initially, the study's magnet work package studied cosine-theta, block-coil, and common-coil type magnets in the framework of the European Circular Energy-Frontier Collider Study (EuroCirCol) H2020 project [2]. Using slightly different assumptions, a fourth option was proposed in [3], called the canted-cosine-theta (CCT) design. In a CCT magnet, the cable is wound around the magnet aperture along a tilted helical path

$$\vec{r}(\theta) = \begin{pmatrix} (-1)^{\ell} R\cos(\theta) \\ R\sin(\theta) \\ \sum_n \frac{B_n}{n B_{\mathrm{ref}}} R^n \sin(n\theta)\cot(\alpha_\ell) + \frac{P\theta}{2\pi} \end{pmatrix}, \quad (1)$$

where ℓ is the layer number, R is the baseline radius, $0 \leq \theta \leq 2\pi n_{\mathrm{turn}}$ is the azimuthal angular position, n_{turn} the number of turns, n the harmonic order, B_n/B_{ref} is the ratio between the n-th desired normal field harmonic and the main or reference harmonic (skew harmonics are not taken into account here), α_ℓ is the baseline's tilt angle in layer ℓ, and P is the tilted helix' twist pitch. A second layer is wound with the same pitch, tilted in the opposite direction. The solenoidal field components of the two layers cancel, and the remaining field in the straight section of the magnet is a purely transverse field with the desired multipole content [4].

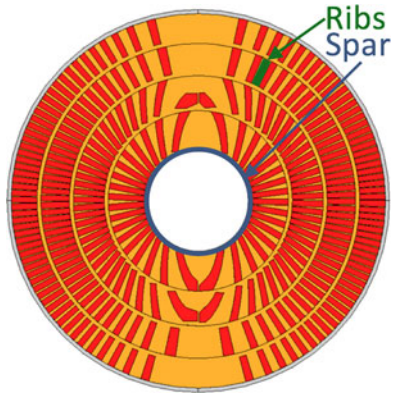

Fig. 1. Schematic cut through the four layers of a coil in the 16-T CCT magnet. Ribs are what separate individual channel turns, and spars are what is left of the full cylinder after machining the channel.

The winding formers (see Fig. 1, right) provide azimuthal and axial stress-management functionality, whereby the respective Lorentz force components are transmitted to the ribs, and from there onto the solid spar; compare Fig. 1. In this way, the impregnated cable is protected from over-compression, and the coil does not need to be axially prestressed. Herein lies one of the main advantages of the CCT design with respect to the other three variants: it promises to provide significant stress margins with respect to even pessimistic predictions of performance-degrading transverse stress levels in Nb_3Sn cable [7], [8].

For a CCT design to be eligible as a competitor in the FCC Design Study, it needs to (a) be proven to be windable, (b) use conductor in amounts comparable to the most efficient magnet designs, (c) have good field quality, (d) keep coil stresses below 150 MPa at room temperature and below 200 MPa in cryogenic conditions, (e) have a sufficiently low inductance for powering in a string of magnets, (f) be protectable. In this paper, we summarize the efforts at the Paul Scherrer Institute (PSI), in collaboration with LBNL and CERN, to create a CCT 16-T design that would follow exactly the design criteria adhered to by the other three design types in the EuroCirCol project [9].

Manuscript received August 25, 2017; accepted November 6, 2017. Date of publication November 13, 2017; date of current version December 8, 2017. This work was supported by the Swiss State Secretariat for Education, Research, and Innovation SERI. *(Corresponding author: Bernhard Auchmann.)*

B. Auchmann is with the CERN, Geneva CH-1211 Switzerland, and also with the Paul Scherrer Institute, Villigen CH-5232, Switzerland (e-mail: bernhard.auchmann@cern.ch).

L. Brouwer and S. Caspi are with the Lawrence Berkeley National Laboratory, Berkeley, CA 94720 USA.

J. Gao, G. Montenero, M. Negrazus, and S. Sanfilippo are with the Paul Scherrer Institute, Villigen CH-5232, Switzerland.

G. Rolando is with the CERN, Geneva CH-1211, Switzerland.

Color versions of one or more of the figures in this paper are available online at http://ieeexplore.ieee.org.

Digital Object Identifier 10.1109/TASC.2017.2772898

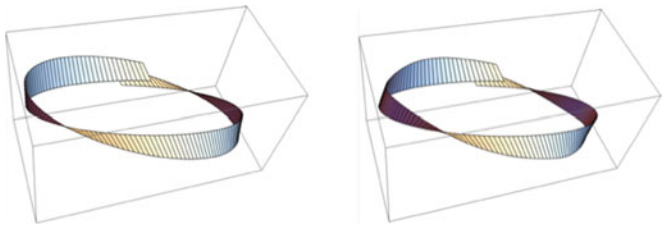

Fig. 2. Left: Conventional CCT winding, with radial cable position above the baseline. Right: Winding scheme optimized for windability and field quality.

In this way, the CCT design can be judged on equal footing in terms of technical- and cost criteria.

In Section II we make some introductory considerations on efficient CCT design. III discusses the question of windability for a high-field CCT magnet. With a solution to this problem, we proceed in Section IV to the 2-D electromechanical design, followed in Section V by 3-D finite-element analysis. Section VI addresses the protection of the proposed CCT design. Section VII discusses efficiency and cost aspects. Finally, Section VIII describes the CCT technology R&D at PSI, geared towards FCC magnets.

II. Efficiency Considerations

An efficient and low-inductance CCT design requires a high effective current density and a small number of turns. Note that there are three mechanisms that lower the effective current density in a CCT with respect to a cosine-theta magnet: (a) the helical winding reduces the obtainable field by a factor $\cos(|\alpha_\ell|)$; (b) the ribs dilute the peak current density on the midplane; (c) the spars dilute the current density on the layers' inner diameters. For all the above reasons, we opt for a four-layer design, using 1.2-mm-diameter strand throughout to reduce the number of ribs and decrease the number of turns. The inner-layer Rutherford cable is 15 mm wide. The minimum rib thickness is reduced to 0.2 mm, which is the smallest thickness proven to be machinable, resulting in a twist pitch of 11 mm, and the spar thickness is set to 2 mm.

III. Windability Studies

Winding a $w = 15$-mm-wide, 2-mm-thick cable in CCT fashion into a channel with $R = 27$ mm inner radius (25 mm free aperture and 2×2 mm spar) is challenging. The conventional CCT design places the cable radially above the baseline (see Fig. 2, left), which leads to a large difference between the lengths of the inner and the outer cable edges, i.e., the cable is torn. For an FCC magnet, with the ratio $\frac{w}{R} = \frac{15}{27} = 0.55$, it is not possible to force a Rutherford cable into this radial position. However, applying the differential-geometry methods of [10], [11], we were able to modify the cable position above the baseline in such a way as to reduce the perimeter difference by a factor ten. The result is displayed in Fig. 2 (right).

The problem that comes with the departure from the conventional, radial cable position above the baseline is that the field quality deteriorates. In our case, a purely mechanical optimization led to 80 units 10^{-4} in relative sextupole. Equation (1) holds the solution to this problem: A variation of the baseline can compensate for the unwanted harmonics, using the parameters B_n, $n \neq 1$. Due to the non-radial cable position, the optimum field quality needs to be found in a simple fixed-point iteration. At this point the mechanical problem needs to be reoptimized, influencing again the field quality. This interdependency between the two optimizations is considered in an outer fixed-point iteration loop, which leads to a global optimum within a few steps.

A winding test was carried out in 2016 at LBNL. The cable position was made to vary smoothly from the optimized position at the onset of the first turn, to the radial position above the baseline in the last turn. A 1.38×22 mm 51-strand Rutherford cable was available for the winding test. The winding test confirmed the theory, in that the optimized turn could be wound without problem, the second turn was still possible, but the Rutherford cable collapsed in every attempt to insert it into the third, radial channel. The test was repeated another three times with different cables, confirming the result.

IV. 2-D Design

A. Electromagnetic Simulation

The 2-D cross-section model of the coil is obtained from a 3-D coil model via bisection algorithm. In 3-D, the hexahedral bricks making up the cable are filled with straight line current segments. In the 2-D cut, these line currents are represented as points. The Biot-Savart law accounts for the coil field. In order to take into account the contribution from the nonlinear iron yoke, the point-current model was coupled to the Finite-Element/Boundary-Element method [12] implemented in the ROXIE software [13].

The electromagnetic optimization of a CCT coil essentially boils down to the choice of a tilt angle (here 15 degrees from the midplane) according to efficiency criteria [4], a cable according to protection and efficiency criteria, and the minimum spar- and rib widths according to mechanical and machinability criteria; see above. The magnetic iron, which is in intimate contact with the coil, introduces low field distortions. Electromagnetic simulation, therefore, serves to check each layer's position on the loadline, as well as to produce field maps for electro-thermal calculations, and Lorentz-force input to the mechanical design.

At nominal current, the simulated field quality, excluding persistent-current effects, is well below one unit 10^{-4} in all relative harmonics b_n for $n > 3$, with a b_2 of six units due to cross-talk between the apertures. The loadline margins are 14% in Layers 1–3, and 16% in Layer 4, which is a necessity in order not to drop below 70% current margin (vertical margin towards the critical surface in the loadline plot). A lower current margin may push the working point into unstable territory.

B. Mechanical Design

In the mechanical design, we start from the CCT-specific premise that neither azimuthal nor axial prestress are needed, as the respective force components are transferred turn-by-turn to the former's ribs and from there to the spar. As for the radial

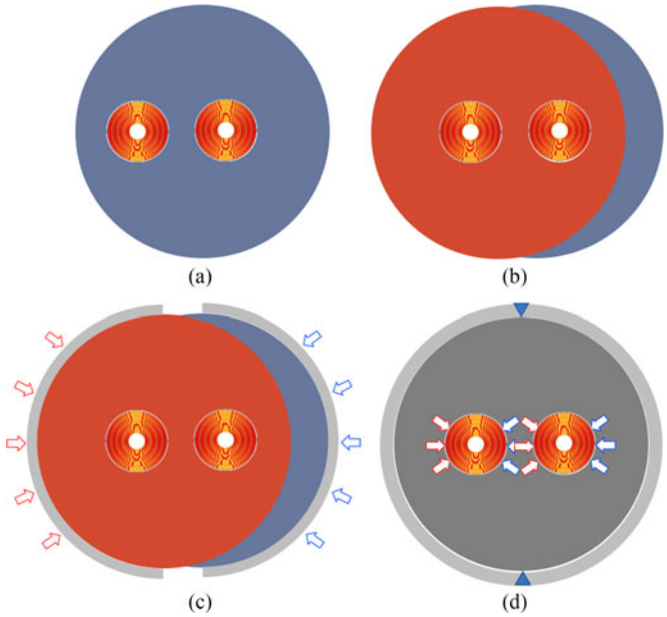

Fig. 3. Scissors lamination schematic explanation: (a) placement of first lamination; (b) flipped second lamination; (c) with half-shells under welding press; (d) welded half shells with weld shrinkage, horizontally pre-loaded coils.

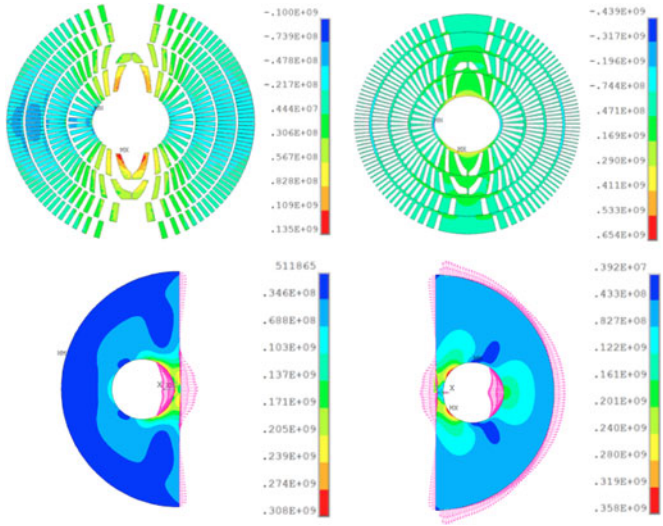

Fig. 4. Top left: Azimuthal stress on the conductor (peak: 135 MPa). Top right: Azimutal stress on the formers (peak: 440 MPa in compression with node-based singularities in extension). Bottom: Von Mises stress in the two layers of yoke lamination (peak: 360 MPa in compression). The left image is the horizontally flipped second yoke layer in the model. The reaction pattern indicates the preloading of the coils.

force component, which tends to ovalize the coil horizontally, the minimal spar thickness chosen for efficiency cannot provide enough stiffness to prevent excessive coil deformation. An external support structure is required to react in particular around the midplane. We adopt the idea of scissors laminations for this purpose [14]: A 1-cm-thick protective iron shell is placed around each of the coils of the twin-aperture magnet, and a single-piece yoke lamination is stacked onto the two coils. The holes for the coils are slightly off-center horizontally (by 0.5 mm) with respect to the nominal coil centers. The laminations are stacked in alternating orientation, as to result in a square-wave pattern on the yoke's outer diameter around the horizontal midplane. The assembly is placed into 25-mm-thick stainless-steel half-shells, which are welded under a welding press. Every second lamination pushes on the coils. The protective shell dilutes peak stresses on the coil (Fig. 3).

The analysis was carried out with ANSYS [15] in plane-stress conditions. The shell thickness of 25 mm is designed to be close to the limit of its mechanical strength (with appropriate margin) at room temperature. This is because it is thought that 25 mm is rather challenging to weld with sufficient weld shrinkage (0.9 mm per half-shell; compare to 0.85 mm achieved in welding trials on 12-mm-thick shells [16]). This amount of weld shrinkage is needed to sufficiently pre-compress the scissor laminations and, consequently, provide radial support to the coils. Material properties and stress limits are taken from the EuroCirCol program [9]. Simulation results are displayed in Fig. 4. The coil stress at nominal field is only 135 MPa, which is a result of the CCT design's azimuthal stress management. The former in the model is made from Al-bronze CuAl7Si2 where we assume a stress limit of 450 MPa. Efforts are currently under way to validate this assumption and characterize the material after a heat treatment at room temperature and in cryogenic conditions.

V. 3-D Analysis

A. Electromagnetic Analysis

For the 3-D electromagnetic analysis, Opera 3-D was used [17]. To achieve "straight-section" conditions in the center of the model, 240 CCT turns were required in the model. It was found that the fields in the magnet ends exceeded the straight-section fields by only 0.02 T. As there are no mechanical discontinuities in the ends of a CCT magnet, this allowed us to extend the yoke over the entire length of the winding former, whereas other design variants cut back the yoke in order to provide additional margins in the coil ends. The magnetic length of the magnet with iron was found to be identical to the magnetic length without iron, which can be calculated from the number of turns and the pitch length by $L_{\mathrm{mag}} = n_{\mathrm{turns}} \times P$. These findings allowed us to compare the difference between the magnet's mechanical length (excluding the electrical connections) and its magnetic length with the same value in a 2-layer cosine-theta design for the High-Luminosity upgrade of the Large Hadron Collider [18]. In both cases, the difference amounts to about 50 cm.

B. Periodic Mechanical Analysis

Since the CCT design does not feature a continuous translational symmetry in between the magnet ends, a 3-D analysis is required to cross-check the 2-D simplification of Section IV-B. The twist pitch, which is 11 mm in all four layers, provides a discrete symmetry in the magnet which can be exploited to analyze the straight section at the level of a discrete slice; see Fig. 5. We use the generalized-plane-stress condition described in detail in [19]. This technique accounts for the axial thermal

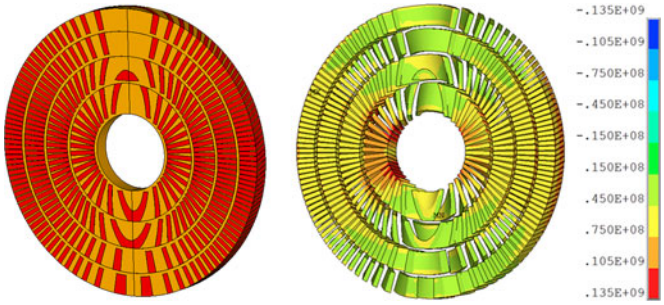

Fig. 5. Left: Single-pitch slice model of the coil. Right: Von Mises stress on the impregnated cable (peak: 135 MPa, neglecting single-node singularities).

shrinkage by assigning a single contraction value to each glued component in the magnet assembly. The individual shrinkage values are determined as to set for each component the integrated axial forces on the front- and back surfaces, respectively, to zero. Fig. 5 shows the slice model of the coils, as well as the stresses on the impregnated cable. The results differ from the 2-D results in Fig. 4 (top left) in the location of the peak stresses, which should be expected given that a 2-D model cannot predict the correct former stiffness. The magnitude of peak stress, however, is consistent with 2-D predictions. Similar observations have been made for the former, whereas the other structural components are in agreement with 2-D.

VI. Electrothermal Analysis

Following the EuroCirCol Project's approach, a simplified protectability study has been an integral part of the design process [20]: it is assumed that 40 ms after the quench initiation (at 105% of nominal current) 100% of the coil is quenched (by either heaters, CLIQ [21], or another protection scheme). An adiabatic integrator calculates both, the hot-spot temperature and the coil resistance, which kicks in after 40 ms to dissipate the magnet's stored magnetic energy. The peak temperature in this analysis must remain below 350 K [9].

The quench analysis was used to find the optimal cable grading, assigning an individual number of strands and copper/non-copper ratio to each layer. As a consequence, the temperature distribution across the coils is rather smooth (see Fig. 6), as compared to that of cosine-theta and block-coil designs [23], which use only two cable types, one for each inner and outer double-pancake coil. The calculation of voltages to ground must be carried out differently than in axially-wound magnets. The sum of inductive and resistive voltage per turn builds up over more than a thousand turns per layer (the FCC dipole magnetic length is 14.3 m). The connectivity between layers must be chosen as to minimize the overall peak voltage to ground.

VII. Cost Efficiency and Other Considerations

Considering all criteria outlined in [9] for the EuroCirCol WP5, the present CCT design requires 9.7 kt of conductor to construct the 4578 magnets of the FCC. This number is 30% higher than the most efficient design options, the cosine-theta and the block coil. Moreover, it must be noted that the manufacturing of the winding former is still considered as a

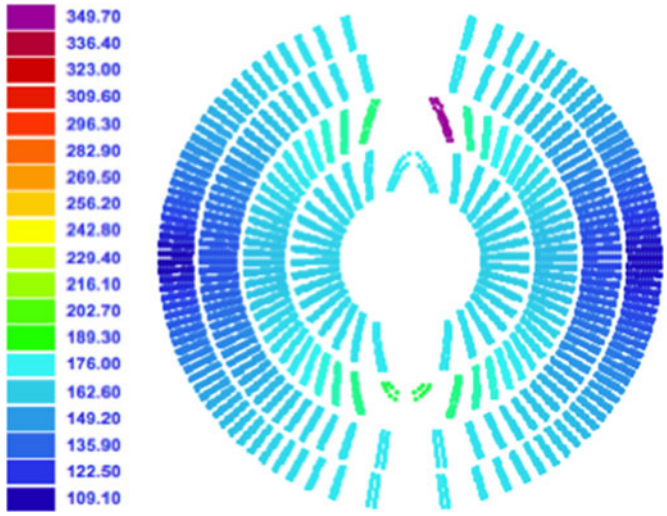

Fig. 6. Temperature profile after a quench in the second-layer.

challenge, technologically and in terms of cost. CNC machining trials have successfully been carried out for the tilted deep channels required in the inner two CCT layers; see Fig. 1. PSI has started a collaboration with the IWS Fraunhofer Institute of Dresden, Germany, for cost-effective CCT-former manufacturing by means of thin laminations [24]. It should be noted, however, that the external mechanical structure of the CCT magnet is simple as compared to the bladder-and-key structures proposed for the competing design options. The number of parts is drastically reduced. The welded shell is economical in both, cost and space requirements. Note that the 16-T bladder-and-key Aluminum shells are about 100 mm thick, and need to be enclosed in a helium-tight steel shell. For this reason, the CCT design is suited as is for the High-Energy LHC (HE-LHC) option, where space requirements are more stringent due to the existing LHC tunnel. Finally, in the context of Section VI, an alternative winding approach should be mentioned: a CCT layer could be wound as a double-helix. Each of the two helices in a given layer would have twice the twist pitch of the single-helix design. The increase in twist pitch would introduce a weak skew dipole field which would have to be corrected in the baseline. In this way, voltages to ground could be cut in half, while reducing to 50% the required conductor unit-length, which may imply important cost benefits, partly or fully compensating the above 30%. The double-helix option will be studied in more detail in the coming year. Overall, we expect that the CCT design can be competitive with other designs in terms of manufacturing cost.

VIII. The PSI CCT Technology Program

As a result of the above findings, a CCT technology program has been set up at PSI for an initial period of three years, in order to study design features specific to a CCT magnet for the FCC main dipole. The PSI program coordinates closely with the CCT R&D under the US MDP program [22], building upon the growing experience with high-field CCT magnets at LBNL, and adding FCC-specific features such as wide cables wound on relatively small radii, thin spars, and a custom-built external

mechanical structure [5]. Two model magnets are foreseen to be built: CD1 (Canted Dipole 1), which uses similar coil technology as the MDP program with reduced spar thickness and an external structure, and CD2, which, in addition to CD1 features, will use a wide cable following the approach outlined in Section III.

IX. Conclusion

We have described a CCT design for the FCC main dipole, which follows all the same design criteria as the EuroCirCol Project's cosine-theta, block-coil, and common-coil options. The design is suitable for both, an FCC main dipole, and an HE-LHC main dipole. It uses more conductor than the other options, in particular cosine-theta and block coils. At the same time it features a much simplified mechanical structure. The design proves that CCT technology can provide important mechanical margins with respect to the degradation limit of Nb_3Sn cables. Whether or not this margin can translate into improved magnet performance is a subject of active R&D at the US MDP program, as well as at the PSI CCT Technology Program. PSI focuses is on the implementation of particular design features that are necessary to make the CCT technology a viable candidate for an FCC or HE-LHC accelerator.

References

[1] D. Tommasini *et al.*, "Status of the 16 T dipole development program for a future hadron collider," submitted for publication.

[2] D. Tommasini *et al.*, "The 16 T dipole development program for FCC," *IEEE Trans. Appl. Supercond.*, vol. 27, no. 4, Jun. 2017, Art. no. 4000405.

[3] S. Caspi, D. Arbelaez, L. Brouwer, S. Gourlay, S. Prestemon, and B. Auchmann, "Design of a canted-cosine-theta superconducting dipole magnet for future colliders," *IEEE Trans. Appl. Supercond.*, vol. 27, no. 4, Jun. 2017, Art. no. 4001505.

[4] L. N. Brouwer, "Canted-cosine-theta superconducting accelerator magnets for high energy physics and ion beam cancer therapy," Ph.D. dissertation, Univ. California–Berkeley, Berkeley, CA, USA, 2015.

[5] G. Montenero *et al.*, "Mechanical structure for the PSI canted-cosine-theta (CCT) magnet program," submitted for publication.

[6] M. Sorbi *et al.*, "The EuroCirCol 16T cosine-theta dipole option for the FCC," *IEEE Trans. Appl. Supercond.*, vol. 27, no. 4, Jun. 2017, Art. no. 4001205.

[7] B. Bordini, P. Alknes, A. Ballarino, L. Bottura, and L. Oberli, "Critical current measurements of high J_c Nb_3Sn Rutherford cables under transverse compression," *IEEE Trans. Appl. Supercond.*, vol. 24, no. 3, Jun. 2014, Art. no. 9501005.

[8] F. J. Wolf *et al.*, "Characterization of the stress distribution on Nb_3Sn Rutherford cables under transverse compression," submitted for publication.

[9] F. Toral *et al.*, "16-T dipole design options: Input parameters and evaluation criteria," EuroCirCol-P1-WP5 version 3, H2020 Grant Agreement 654305, Jun. 2016.

[10] B. Auchmann and S. Russenschuck, "Coil end design for superconducting magnets applying differential geometry methods," *IEEE Trans. Magn.*, vol. 40, no. 2, pp. 1208–1211, Mar. 2004.

[11] B. Auchmann, S. Russenschuck, and N. Schwerg, "Discrete differential geometry applied to the coil-end design of superconducting magnets," *IEEE Trans. Appl. Supercond.*, vol. 17, no. 2, pp. 1165–1168, Jun. 2007.

[12] S. Kurz and S. Russenschuck, "Numerical simulation of superconducting accelerator magnets," *IEEE Trans. Appl. Supercond.*, vol. 12, no. 1, pp. 1442–1447, Mar. 2002.

[13] S. Russenschuck *et al.*, ROXIE. [Online]. Available: http://cern.ch/roxie. Accessed on: Aug. 2017.

[14] A. Ijspeert and J. Salminen, "Superconducting coil compression by scissor laminations," in *Proc. Particle Accel. Conf.*, Barcelona, Spain, Jun. 1996. [Online]. Available: http://jacow.org

[15] ANSYS, Inc., Canonsburg, PA, USA, Ansys 17.0. [Online]. Available: http://www.ansys.com. Accessed on: Aug. 2017.

[16] F. Lackner, "Welding trials," presented at the 11-T Dipole Informal Coil Assembly Readiness Review, Geneva, Switzerland, Sep. 2013. [Online]. Available: http://indico.cern.ch/event/273023

[17] Cobham Technical Services, Kidlington, U.K., Opera Simulation Software. [Online]. Available: http://operafea.com. Accessed on: Aug. 2017.

[18] F. Savary, "The 11T dipole magnet for HL-LHC," presented at the Holland@CERN Meeting, Geneva, Switzerland, Jun. 2016. [Online]. Available: https://indico.cern.ch/event/539240

[19] L. N. Brouwer, D. Arbelaez, S. Caspi, H. Felice, S. Prestemon, and E. Rochepault, "Structural design and analysis of canted-cosine-theta dipoles," *IEEE Trans. Appl. Supercond.*, vol. 24, no. 4, Jun. 2014, Art. no. 4001506.

[20] T. Salmi *et al.*, "Quench protection analysis integrated in the design of 16T Nb_3Sn dipoles for the future circular collider," *Phys. Rev. Accel. Beams*, vol. 20, no. 3, 2017, Art. no. 032401.

[21] E. Ravaioli, "CLIQ: A new quench protection technology for superconducting magnets," Ph.D. dissertation, Univ. Twente, Enschede, The Netherlands, 2015.

[22] S. Prestemon, "The U.S. magnet development program for high field accelerator magnet R&D," submitted for publication.

[23] T. Salmi *et al.*, "Validation of quench protection simulations in high-field Nb_3Sn magnets by comparison with measurements," submitted for publication.

[24] A. Techel, "Lamellierte werkzeuge im formen- und werkzeugbau – metal laminated tooling (MELATO)," *Werkstattstechnik Online*, vol. 94, no. 11–12, 2004. [Online]. Available: http://www.springer-vdi-verlag.de/libary/news/2004/10/WBK_4_11_MELATO.pdf